Applied Chemical Engineering (2025) Volume 8 Issue 2 ISSN: 2578-2010 (O)
doi: 10.59429/ace.v8i2.5703

RESEARCH ARTICLE

Adsorption of doxorubicin- hydrochloride onto garlic-loaded chitosan-poly (acrylic acid)/MWCNTs nanocomposite

Mohammed A. Kadhim [1*], Zeina M. Kadam[2]

[1*] *Department of Science, College of Basic Education, Al-Muthanna University, Samawah, 66001,Iraq*

[2] *Department of chemistry, College of Science, Al-Qadisiyah University, Diwaniyah, 58001,Iraq*

***Corresponding author:** Mohammed A. Kadhim; mohammed.kadhim.isa@atu.edu.iq

ABSTRACT

This study details the synthesis of a bioactive nanocomposite material designed for drug delivery. It was synthesized using chitosan (CS), multi-walled carbon nanotubes (MWCNTs), acrylic acid (AA), and garlic powder (GAR) through free radical polymerization. The primary goal was to assess its effectiveness in removing the anticancer drug Doxorubicin hydrochloride (DOX-HCl) from aqueous solutions. The resulting nanocomposite, (CS-co-PAA-GAR/MWCNTs), was thoroughly characterized using FTIR, XRD, FESEM, TEM, BET, BJH, and AFM techniques. The adsorption of DOX-HCl onto the nanocomposite was evaluated using the Langmuir, Freundlich, and Temkin isotherm models. Results showed strong and desirable adsorption, indicated by a Freundlich isotherm constant (KF) of 1.08 (mg g-1 (mg L-1)-1/n) and a separation factor of 0.9904. Optimal adsorption occurred at a DOX-HCl concentration of 100 mg/L, a temperature of 293 K, and a pH of 6. A significant finding was that increasing the pH level reduced DOX-HCl adsorption and caused dehydrogenation. Furthermore, the Van't Hoff equation revealed that DOX-HCl adsorption exhibited fast kinetics, with a negative thermodynamic ΔH of -9.0381 kJ/mol. This was confirmed by the excellent fit to pseudo-second-order kinetic model (R2 = 0.9997). These findings collectively demonstrate that synthesized nanocomposite effectively removes DOX-HCl from aqueous solutions.

Keywords: Anticancer drug; DOX-HCl; Garlic powder, Hydrogel; MWCNTs, Adsorption

ARTICLE INFO

Received: 1 June 2025
Accepted: 13 June 2025
Available online: 30 June 2025

1. Introduction

Researchers are looking into a new technical strategy that uses intracellular agents, like nanoparticles, to get around problems with the current radiation and chemotherapy treatments for cancer. Nanocomposites are used in many different applications and are growing in popularity. In the meantime, the use of nanocomposites in medical procedures has increased. The use of nanocomposites as a drug delivery system for cancer treatment is one of the real-world uses of nanotechnology currently being explored. These systems, which usually include a drug, a coating or carrier, and targeting factors, are made to guarantee that the drug is released under controlled circumstances, that its concentration stays within a therapeutic range for the necessary duration, and that the drug is delivered precisely to the target tissue [1-3]. Chemo-drugs have recently been incorporated into a variety of nanoparticle-based drug delivery systems [4-7]. Numerous nanomedicines, including inorganic nanoparticles and viral nanoparticles [8], as well as lipid-based, natural, or synthetic polymer-based nanocarriers, are currently being studied in clinic for cancer therapy [9]. Solid tumors, transplantable leukemia, and lymphomas are

among the cancers that can be treated with doxorubicin hydrochloride (DOX), a naturally occurring ring anthracycline derivative [10]. Usually used in combination with cyclophosphamide, vincristine, bleomycin, or prednisone, it is an essential part of multi-chemotherapeutic drug regimens [10, 11].

In daily life, garlic (*Allium sativum L.*) is used as an herbal remedy and flavoring ingredient. Among the many benefits of garlic are its anti-tumor, antioxidant, immune-boosting, and cardiovascular disease prevention and treatment properties [12]. Sulphides (allicin), amino acids, polysaccharides, polyphenols, vitamins, and minerals are among the many nutrients and useful ingredients found in garlic [13]. Related products include pickled garlic, black garlic, preserved garlic, aged garlic extract, garlic powder, and garlic essential oil [14-16]. A large portion of these products is dried garlic. Garlic is widely known for its antiseptic, antifungal, and anti-inflammatory properties [17]. The potential medical benefits of garlic have been demonstrated in contemporary medicine, including lowering blood pressure, preventing cardiovascular and cerebrovascular diseases, promoting liver function, improving glucose metabolism, antibacterial activity, antioxidant and anti-aging, antitumor, and antiviral properties [18-24]. Researchers also suggested that thio-sulfinate molecules, particularly diallyl thio-sulfonate (allicin) and S-allyl-cysteine sulfoxide (alliin), are the main bioactive components of garlic [25]. Additionally, about 70 % of active ingredients in garlic are allicin, which may have an antioxidant effect on the body because of its sulfonyl [26-28]. The inherent antioxidant and anti-tumor properties of garlic, particularly through compounds like allicin, present a compelling opportunity to synergize with conventional chemotherapeutics like doxorubicin. By incorporating garlic-derived components, it is hypothesized that the overall therapeutic efficacy of DOX can be enhanced, potentially reducing its toxic side effects through the attenuation of oxidative stress, and even overcoming drug resistance mechanisms. This combinatorial approach leverages the strengths of both synthetic drugs and natural bioactives within a targeted delivery system. In this study, we worked on the synthesis of MWCNTs/hydrogel nanocomposite, stabilized it with rosemary to increase adoption efficiency, and used in the form of nanocomposite of CS-co-pAA-GAR and MWCNTs to deliver the anticancer drug DOX-HCl to target area.

2. Materials and methods

2.1. Materials

The Garlic came from one of Iraq's herbal factories. All starting materials and solvents that were used in the synthesis of the target compounds were supplied from available sources and were directly used without further purification. Multi-walled carbon nanotubes (MWCNTs) powder (5 g, outer diameter (OD) = 40 to 60 nm, 5–10 μm, 99.0% purity, surface area > 200 m^2/g, layers = 7, density = 2.1 g/cm3) was obtained from VCN Materials, Co., Ltd, Iran. chitosan (CS) (medium molecular weight, 96%) was purchased from HIMEDIA. MACLIN from China provides OFL. Acrylic acid was purchased from Merck, Germany. Acetic acid 99.5% and N, N' methylenebisacrylamide (MBA, 99.0%) as cross-linkers were purchased from CDH, India. The initiator is potassium persulfate (KPS, 99.0%), supplied by Thomas Baker, India. Calcium chloride, sodium chloride, sodium hydroxide, potassium chloride, and hydrochloric acid were supplied from Fluka, Germany. All solutions were prepared by using deionized water (DI).

2.2. Preparation of CS-co-pAA-GAR/ MWCNTs nanocomposite

The preparation process (**Figure 1**) began by mixing 0.5 g of chitosan (CS) with 20 mL of 1% acetic acid to prepare a 2.5 weight percent chitosan solution. This solution was then agitated for 15 minutes at 60 °C to ensure complete chitosan polymer dispersion. Subsequently, a 0.1% MWCNT solution, pre-treated with an ultrasonic field for 10 minutes, was introduced to the CS solution. Grafting was completed by swirling the CS/MWCNTs mixture at 70 °C. During this step, CS macromolecules adsorbed onto the surface of the MWCNTs, effectively acting as a polymeric cationic surfactant and stabilizing them [29]. Ten milliliters of acrylic acid (AA) were then added to the preceding solution, which served as a monomer. Following this, 0.02

g of KPS (in 2 mL deionized water) and 0.02 g of the cross-linker MBA (in 2 mL deionized water) were introduced. The solution was continuously stirred and bubbled with nitrogen for 15 minutes to eliminate oxygen. Next, the mixture was combined with garlic plant powder (GAR). This involved dissolving 0.1 g of garlic powder in 20 mL of deionized water and stirring on a magnetic stirrer for 30 minutes. The solution was then subjected to an ultrasonic apparatus for further dissolution. The plant extract was subsequently added dropwise, and the entire combination was finally transferred to a water bath. The resulting nanocomposite was cut into 5 mm pieces and rinsed repeatedly with deionized water, with water changes every hour for 24 hours, to remove any unreacted monomers. After thorough washing, the nanocomposite was dried to a consistent weight at 60 °C. The synthesized (CS-co-pAA-GAR/MWCNTs) nanocomposite was then crushed, sieved, and stored in airtight containers for later usage [30, 31]. Deionized water served as the solvent throughout the preparation process.

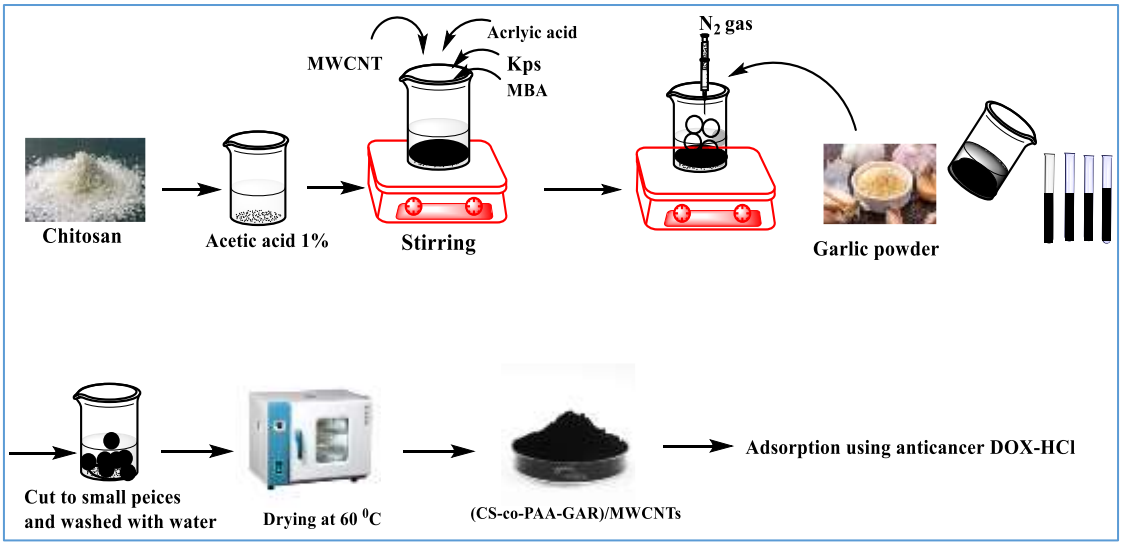

Figure 1. Graphical synthetic route of CS-co-PAA-GAR/MWCNTs nanocomposite

2.3. Characterization

Various analytical techniques were employed to characterize the materials before and after loading with doxorubicin hydrochloride (DOX-HCl). Fourier Transform Infrared (FTIR) spectroscopy was performed using a Bruker Equinox 55, Tensor 27 instrument (Germany) with KBr pellets, capturing spectra in the range of 400−4000 cm^{-1}. X-ray diffraction (XRD) patterns were collected using a Philips PW1730 diffractometer (USA). For microscopic examination, Field Emission Scanning Electron Microscopy (FESEM) was conducted using a Tescan Mira3 instrument (Czech Republic), while Transmission Electron Microscopy (TEM) images were obtained with a Philips EM208S (Netherlands). Nitrogen adsorption-desorption isotherms were measured using a BEL Belsorp mini II device (Japan) to determine surface area via the Brunauer-Emmett-Teller (BET) method. Finally, Atomic Force Microscopy (AFM) was carried out with an Ntegra NT-MDT instrument (Ireland).

2.4. Adsorption isotherms

Batch adsorption studies were conducted to gather preliminary data and establish optimal parameters for drug removal effectiveness. Key variables investigated included drug concentration, equilibrium time, temperature, ionic strength, and pH. For these experiments, 10 mL of a 100 mg/L DOX-HCl solution and 0.05 g of the nanocomposite were used in separate conical flasks. The mixtures were then shaken at 140 rpm until equilibrium was reached, after which they were centrifuged at 4000 rpm for 10 minutes. The drug's adsorption capacity was calculated using a specific equation, and calibration curves were employed to determine the equilibrium concentration using Equation 1 [32-35]:

$$Qe\ or\ \frac{x}{m} = \frac{V(Co-Ce)}{m} \quad (1)$$

The efficiency of drug adsorption (E%) is determined using the Equation 2 [36-39]:

$$E\% = \frac{(Co-Ce)}{Co} \times 100 \quad (2)$$

Where: C_o (mg.L^{-1}) and C_e (mg.L^{-1}) stand for the starting and equilibrium drug concentrations, respectively, and x is the amount of drug adsorbed, whereas m (g) is the mass of the adsorbent material. Qe (mg.g^{-1}) is the amount of drug adsorbed at equilibrium.

3. Results and discussion

3.1. Characterization of CS-co-pAA-GAR/ MWCNTs nanocomposite

Figure 2 depicts FTIR spectra of nanocomposite (CS-co-PAA-GAR/MWCNTs) before (a) and after (b) loading Doxorubicin hydrochloride (DOX-HCl). Spectrum (a) shows peaks for hydroxyl and amine groups at 3400-3500 cm^{-1}, carbonyl (C=O) at 1716 cm^{-1}, and C-H and C-O vibrations. The band near 2600 cm^{-1} may correspond to overtone or combination vibrations often related to carboxylic acid dimers or absorbed moisture, while the broad signal near 3750 cm^{-1} can be associated with free –OH stretching vibrations, typically arising from non-hydrogen bonded hydroxyl groups or residual water [40-42]. As demonstrated in spectrum (b), loading DOX-HCl causes many spectral changes, including the loss or shift of some peaks, particularly carbonyl group, and the development or strengthening of additional peaks. These alterations show that DOX-HCl was successfully loaded onto the nanocomposite via hydrogen bonding or ionic interactions with functional groups in the hydrogel matrix [31,41,43,44].

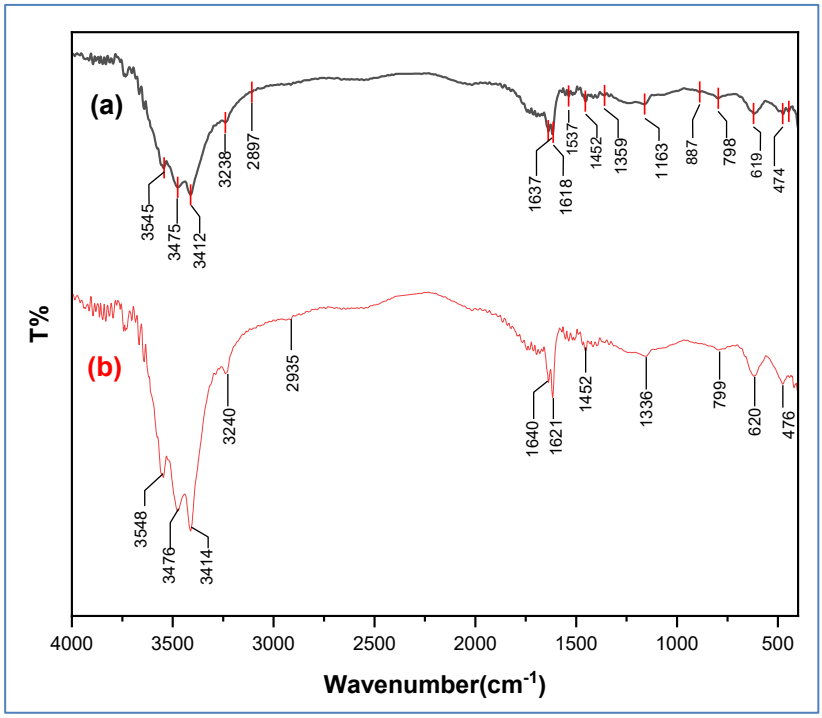

Figure 2. FTIR of CS-co-PAA-GAR/MWCNTs nanocomposite (a) before (b) after loading DOX-HCl

As depicted in **Figure 3a-b,** the X-ray diffraction (XRD) pattern of CS-co-PAA-GAR/MWCNTs nanocomposite, both before (a) and after (b) doxorubicin hydrochloride (DOX-HCl) loading, revealed a prominent peak at 19.542°, indicating its amorphous nature [36, 45]. The significant diffraction observed at 36.592° is attributable to the presence of polyacrylic acid. Upon DOX-HCl loading, the primary peak subtly shifted to 18.792°, and a new broad band appeared at 35.942°. This suggests that the drug is well-dispersed within the polymeric matrix without inducing significant crystallinity [31, 39, 40, 42].

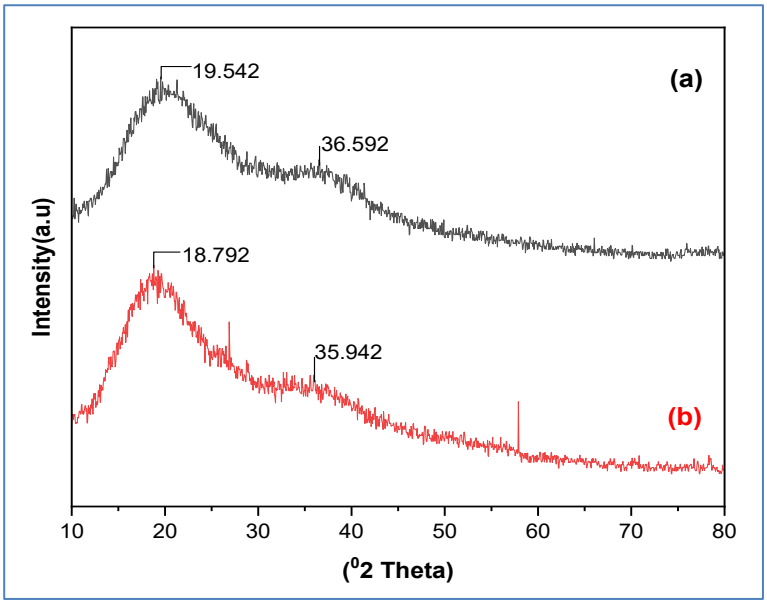

Figure 3. XRD of nanocomposite (CS-co-PAA-GAR/MWCNTs) (a) before (b) after loading DOX-HCl

Figure 4 (a-d) depicts SEM images of CS-co-PAA-GAR/MWCNTs nanocomposite before and after Doxorubicin hydrochloride loading. The surface of composite has a rough, non-smooth texture, which enhances its specific surface area. Additionally, porosity is visible on surface of CS-co-pAA-GAR/MWCNTs nanocomposite, resulting in better adsorption properties [45, 46].

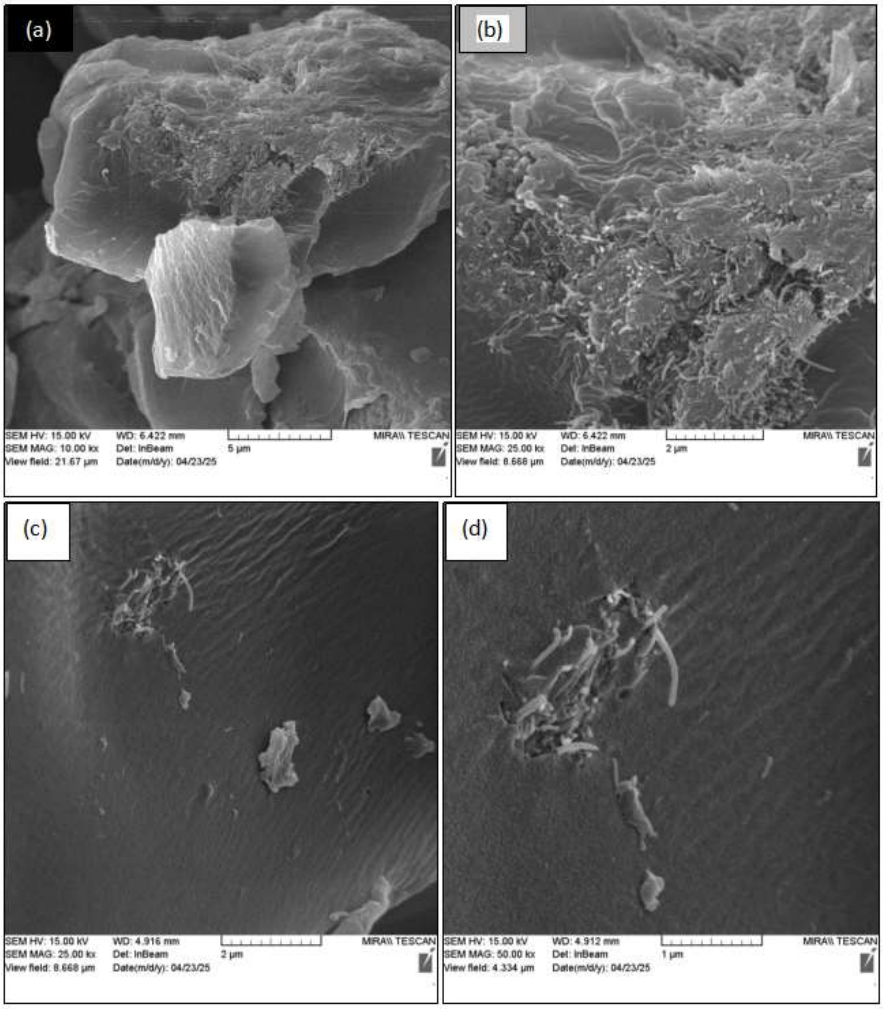

Figure 4. FESEM micrographs of CS-co-PAA-GAR/MWCNTs nanocomposite (a,b) before and (c,d) after DOX-HCl loading

Transmission Electron Microscopy (TEM) micrographs of CS-co-pAA-GAR/MWCNTs nanocomposite, both before and after DOX-HCl loading, are presented in **Figure 5 (a-d).** Notably, individual MWCNTs are not distinctly discernible in these images, suggesting a high degree of homogeneity and a significant impact of chitosan on the carbon nanotubes. The micrographs clearly depict a porous, hollow structure with irregularly shaped particles and distinct lines of aligned pores. This morphology indicates a highly porous architecture and a large specific surface area for the composite. Both SEM and TEM analyses collectively reveal the composite's amorphous nature and provide crucial insights into its overall structure [47].

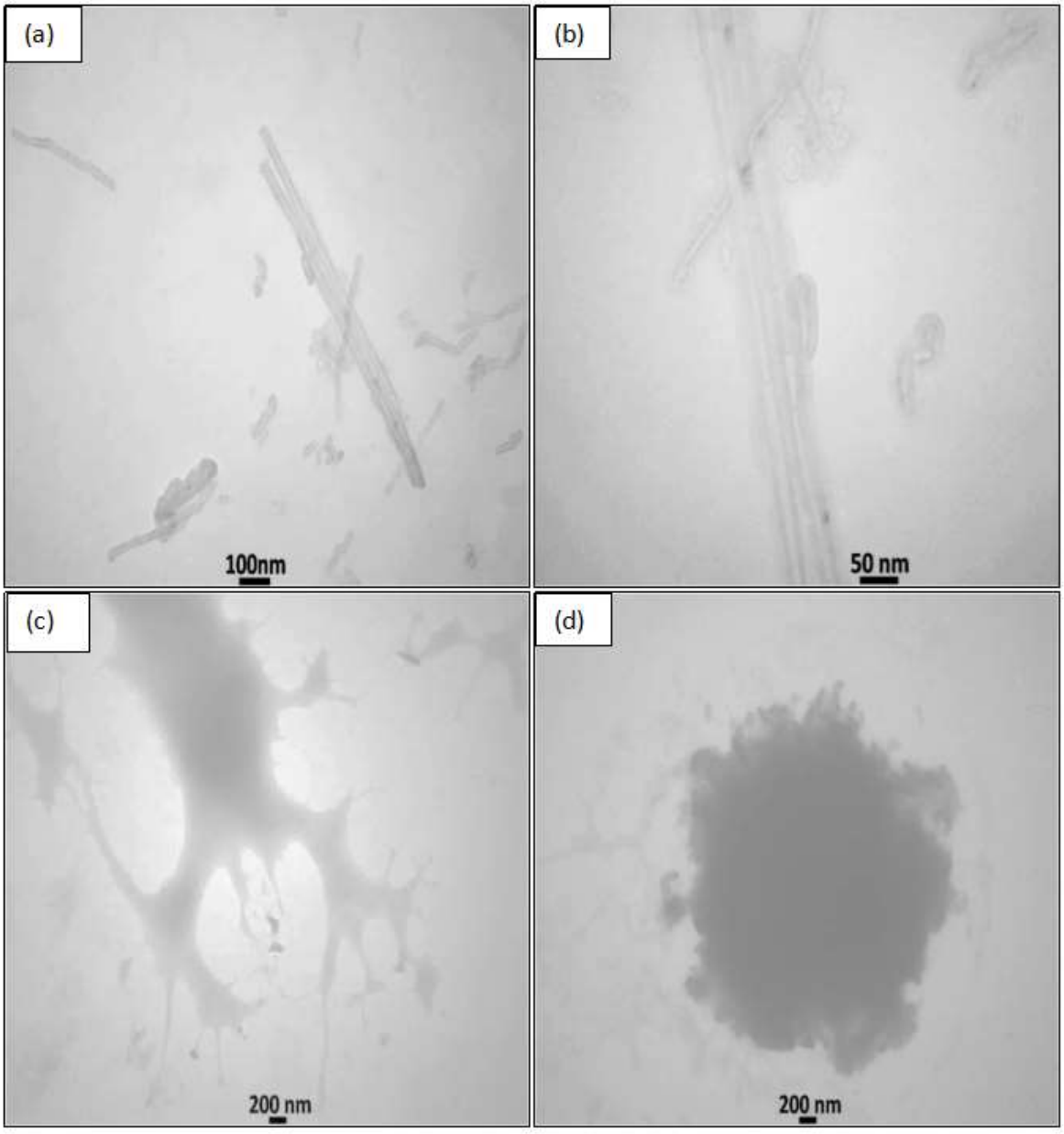

Figure 5. TEM micrographs of CS-co-PAA-GAR/MWCNTs nanocomposite (a,b) before and (c,d) after DOX-HCl loading.

The BET surface area of CS-co-pAA-GAR/MWCNTs (**Figure 6a-d**) was found to be 19.349 m^2/g and an average pore diameter of 9.9992 nm (BJH model). The surface area and average pore diameter of DOX-HCl were reported to be 7.0771 m^2/g and 52.986 nm, respectively. Compared to CS-co-pAA-GAR/MWCNTs before loading drug, the pore size was lower and surface area were large of DOX-HCl, including the drug within the composite matrix, which was likely responsible for this result. **Table 1** shows the result of BET analysis [31].

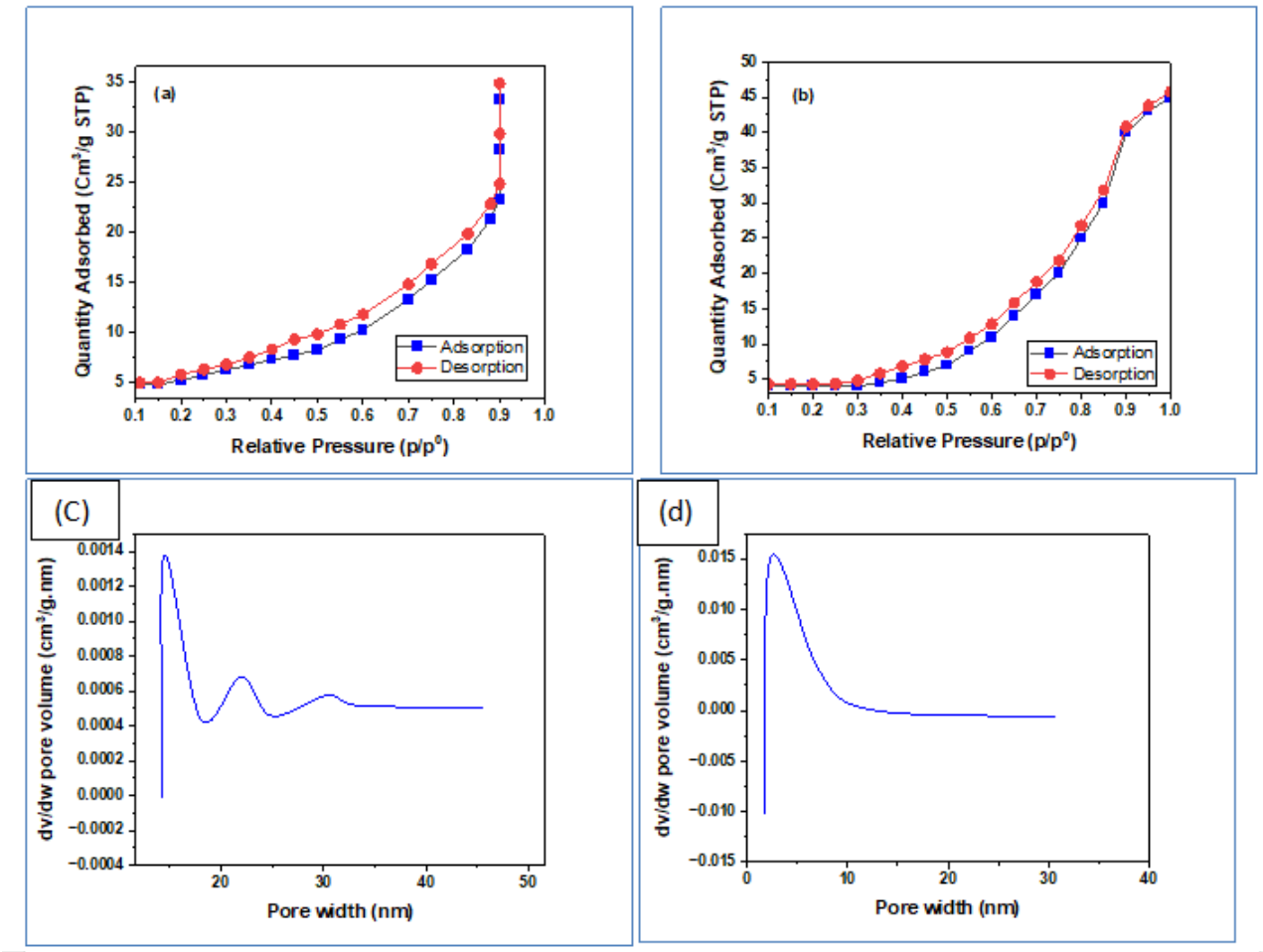

Figure 6. The BET, BJH (a,c) and (b,d) for (CS-co-pAA-GAR/MWCNTs) before and after loading DOX-HCl respectively

Table 1. The BET, BJH for CS-co-pAA-GAR/MWCNTs before and after loading DOX-HCl

(CS-co-pAA-GAR/MWCNTs)	Surface area (m^2/g)	Average pore volume (cm^3/g)	Average pore diameter (nm)
Before loading	19.349	0.048369	9.9992
After loading	7.0771	0.093747	52.986

Figure 7 and **Table 2** show three-dimensional AFM images before (a) and after (b) loading of the DOX-HCl on CS-g-PAA-GAR/MWCNTs nanocomposite. The AFM images reveal two main components; one exhibits numerous peaks extending to tips of carbon nanotubes. This observation indicates a difference in the arrangement of the carbon nanotubes within the relatively rougher nanocomposite matrix due to the addition of garlic powder in the hydrogel formulation [31, 44].

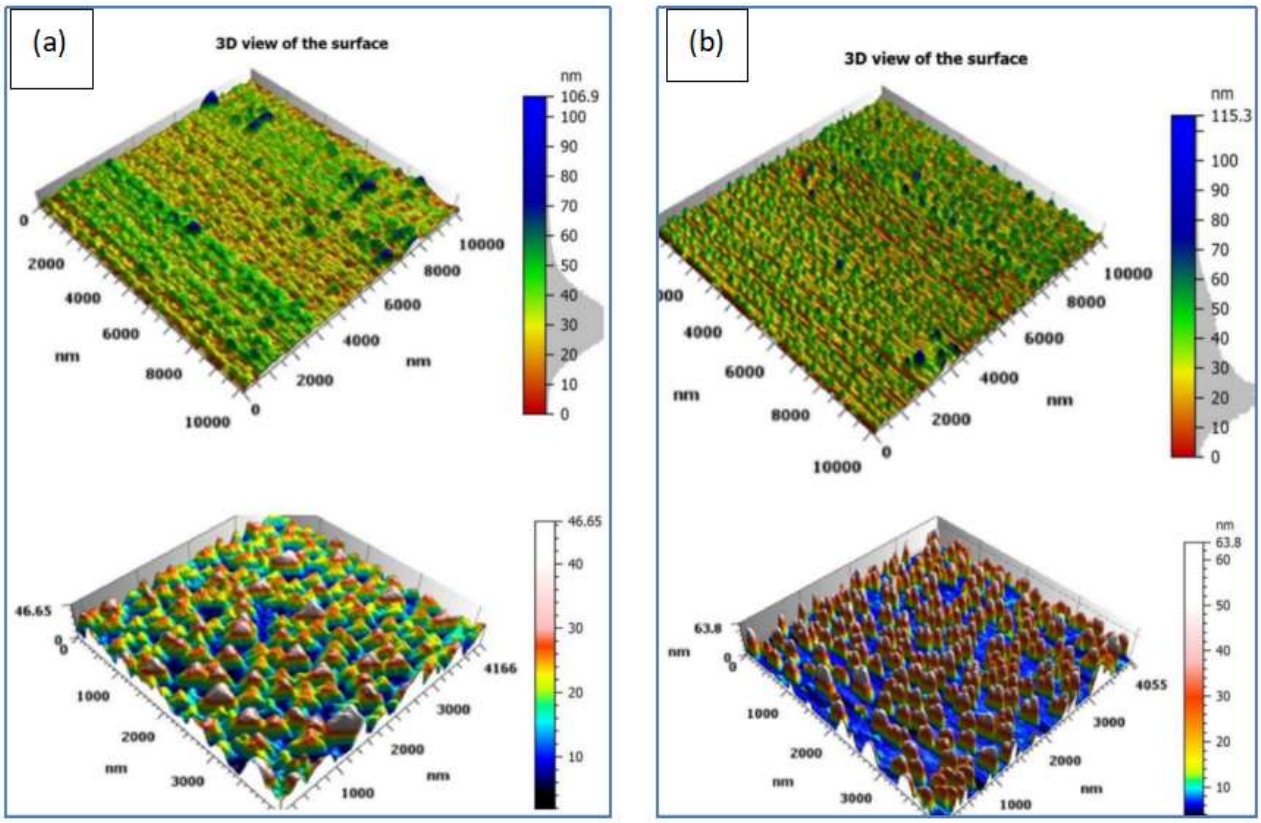

Figure 7. AFM topography of CS-co-PAA-GAR/MWCNTs (a) before and (b) after loading of DOX-HCl

Table 2. The AFM topography for CS-co-pAA-GAR/MWCNTs before and after loading of DOX-HCl

CS-co-PAA-GAR/MWCNTs	Sa	Sq	Ssk	Sku	Sp	Sv	Sz
Before loading	7.784	10.32	0.998	6.292	74.55	32.36	106.9
After loading	11.12	13.92	0.888	3.593	87.13	28.14	115.3

3.2. Adsorption study

3.2.1. Calibration curve of doxorubicin-hydrochloride (DOX-HCl) drug

The DOX-HCl medication was serially diluted to prepare solutions with varying drug concentrations. The absorbance of these DOX-HCl solutions was then measured at 497 nm (λ_{max}) using a sophisticated Shimadzu PC 1800 ultraviolet-visible spectrophotometer. As depicted in **Figure 8,** a strong linear relationship was observed between these absorption values and their corresponding DOX-HCl concentrations. This linearity not only illustrates the direct relationship between concentration and absorption but also confirms the applicability of Beer-Lambert's law within this concentration range. Consequently, a robust DOX-HCl calibration curve can be reliably generated.

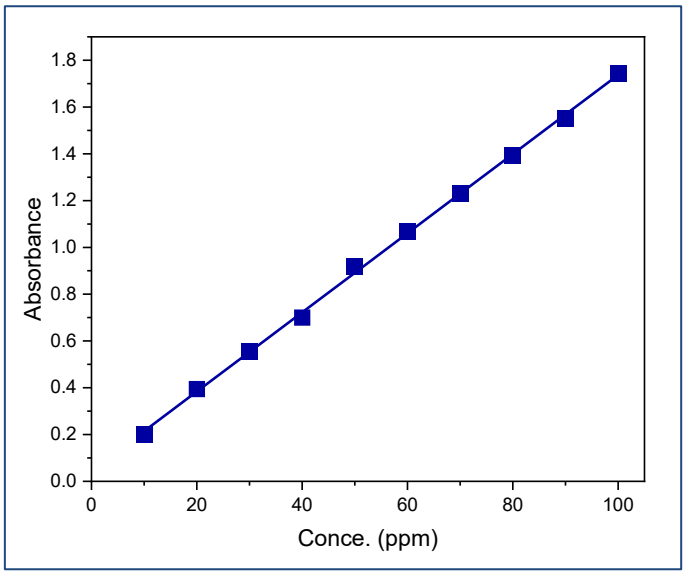

Figure 8. Calibration curve of DOX-HCl drug

3.2.2. Effect of time

Figure 9 illustrates the influence of contact time on the adsorption of medicine by CS-co-pAA-GAR/MWCNTs nanocomposite. During the initial 10 minutes, amount of adsorbed drug rapidly increases, indicating swift utilization of all active sites on adsorbent material. Following this initial period, adsorption rate gradually rises until it reaches a plateau. Based on these observations, optimal adsorption time for drug with CS-co-pAA-GAR/MWCNTs nanocomposite was determined to be 90 minutes, as only a minimal change in amount of adsorbed drug was observed beyond this point [48]. d

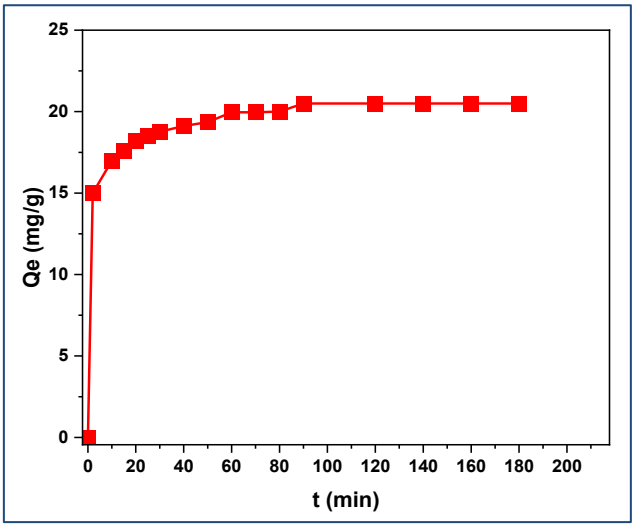

Figure 9. The effect of contact time on DOX-HCl adsorption

3.2.3. Effect of temperature

The impact of temperature on drug adsorption was investigated using DOX-HCl concentrations from 10 to 100 mg/L, with a contact time of 90 minutes, across a temperature range of 15 to 30 °C. As illustrated in **Figure 10,** the results indicate that the adsorption process is exothermic. Specifically, a decrease in temperature led to an increase in the amount of DOX-HCl adsorbed. This suggests that at lower temperatures, the molecules may have less kinetic energy, thereby increasing their likelihood of interacting with the adsorbent. Notably, the amount of DOX-HCl adsorbed remained reasonable when compared to ambient temperatures, with no discernible decrease in adsorption observed from 15 to 30 °C [31, 49, 50].

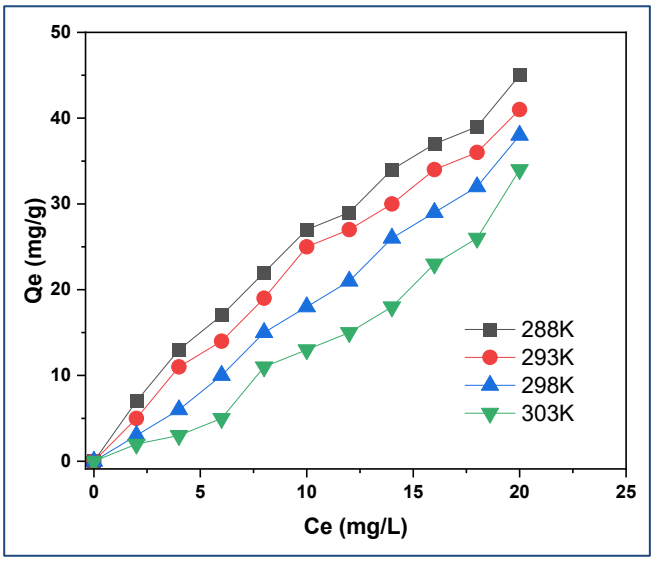

Figure 10. Temperature-related effects on adsorption of DOX-HCl

3.2.4. Effect of pH

The CS-co-pAA-GAR)/MWCNTs nanocomposite demonstrated efficient removal of DOX-HCl across a pH range of 2 to 12, using solutions containing 0.1 mol/L HCl and 0.1 mol/L NaOH. The results are presented in **Figure 11.** DOX-HCl removal efficiency increased from pH 2 to pH 7, peaking at pH 6. This optimal removal at pH 6 is attributed to the ionization of the adsorbate, leading to a negative charge. The combined positive charges of polyacrylic acid and chitosan contribute to electrostatic interactions with drug. Polyacrylic acid contains carboxyl groups (−COOH), while chitosan possesses amino groups ($-NH_2$). Under acidic conditions, the amino groups ($-NH_2$) of chitosan become protonated to form $-NH_3^+$, and the carboxyl groups ($-COO^-$) of poly (acrylic acid) may also become protonated to form −COOH or, under highly acidic conditions, $-COOH_2^+$. These protonated groups remain associated with the polymer backbone and contribute to electrostatic interactions with the negatively charged drug molecules. The relevant equilibria are:

$$-NH_2 + H^+ \rightleftharpoons -NH_3^+ \; ; \; -COO^- + H^+ \rightleftharpoons -COOH$$

Furthermore, the pK_a of primary amine group in DOX-HCl is approximately 8.3 to 9.9, depending on environment. As pH increases above this value, the protonated amine ($–NH_3^+$) begins to deprotonate, reducing electrostatic attraction with adsorbent [31, 33, 51, 52].

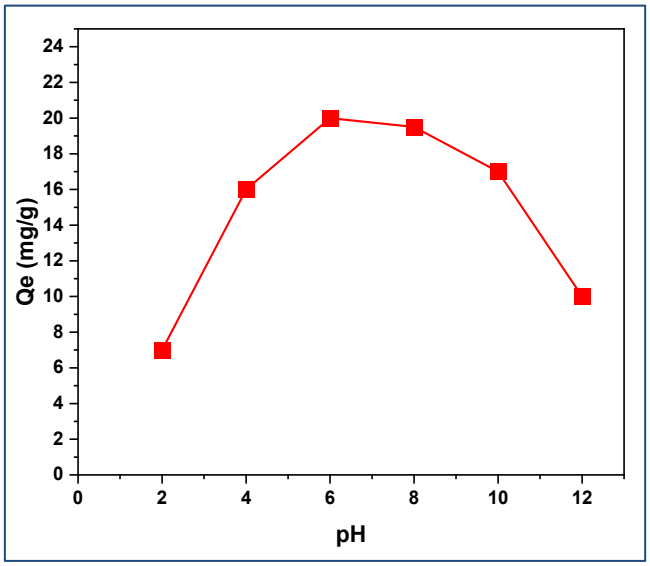

Figure 11. Effect of pH in DOX-HCl adsorption

3.2.5. Effect of ionic strength

Figure 12 illustrates that an increase in salt concentration leads to a decrease in amount of adsorbed material. One explanation for this phenomenon is competition between cationic drug molecules and salt ions for active sites on adsorbent. During adsorption, electrostatic forces typically draw the adsorbent and adsorbate closer; however, with increased salt concentration, this interaction becomes less effective. Additionally, the presence of salt can create a secondary layer that hinders the drug from adhering to the surface [53]. Among the ions tested, the calcium ion exhibits less of an effect compared to others, likely due to its smaller ionic radius. Furthermore, the electrostatic attraction between potassium and sodium ions and nanocomposite's surface can slow down the overall adsorption process.

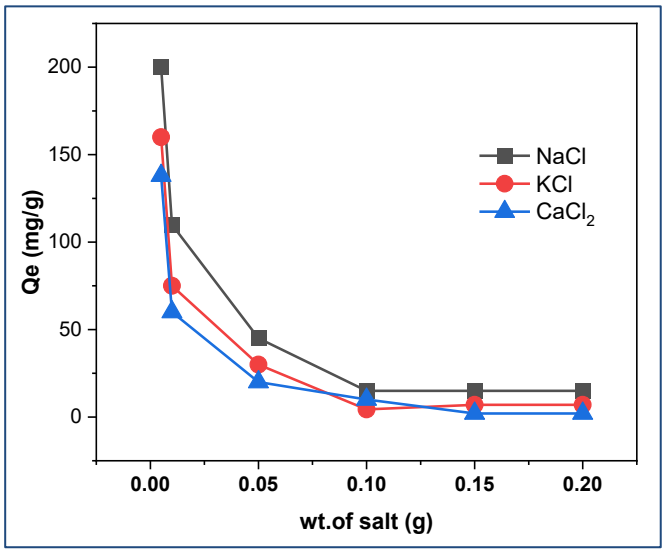

Figure 12. Effect of ionic strength on DOX-HCl adsorption

3.3. Adsorption isotherm models

Adsorption isotherms illustrate the relationship between the adsorbate concentration in a solution and the amount of material adsorbed at a constant temperature [72]. To analyze the adsorption equilibrium data, the Langmuir, Temkin, and Freundlich isotherm models are typically employed. A linear relationship is usually sought, and the applicability of each isotherm equation is assessed using its correlation coefficient. The Freundlich isotherm demonstrates a direct linear relationship between $\log C_e$ and $\log Q_e$. As shown by the correlation coefficient in **Figure 13a-c** and **Table 3,** the ions of the DOX-HCl medication follow the Freundlich isotherm. This finding suggests that the adsorption active sites on the nanocomposite's surface are heterogeneous, exhibiting different energy levels and indicating multilayer adsorption. In contrast, the Langmuir adsorption isotherm describes the formation of a monolayer of adsorbate molecules on a surface with an equal number of available adsorption sites [29, 54-58].

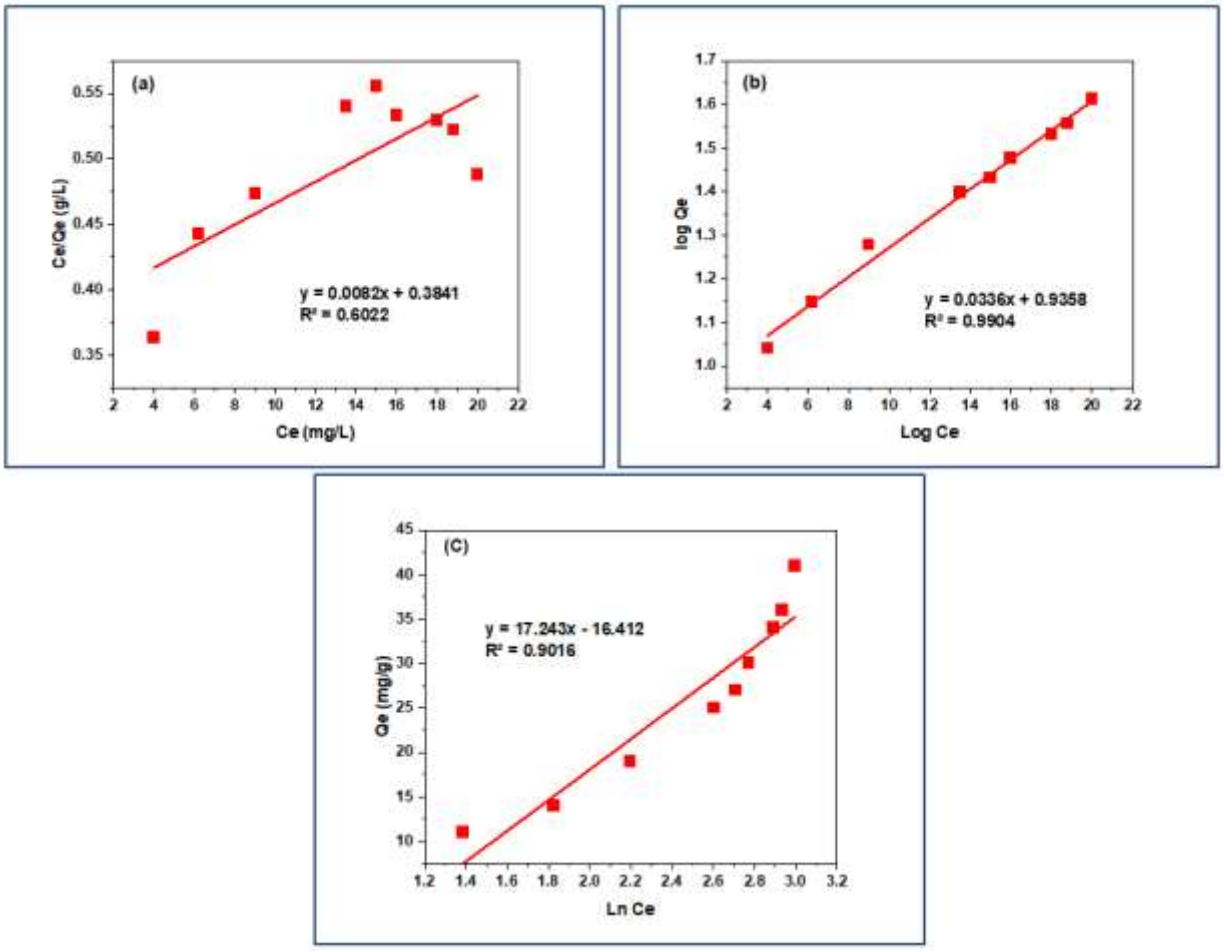

Figure 13. Adsorption isotherms (a) Langmuir, (b)Freundlich and (c)Temkin models

Table 3. The Langmuir Freundlich and Temkin correlation coefficients and constants of DOX-HCl adsorption

Langmuir			Freundlich			Temkin		
K_L (L/mg)	q_{max} (mg/g)	R^2	K_F (mg g^{-1} (mg L^{-1})$^{-1/n}$)	n	R^2	K_T (L/mg)	B (J/mol)	R^2
46.84146	121.9512	0.6022	1.08	29.7619	0.9904	0.386	17.243	0.9016

3.4. Adsorption thermodynamics

The fundamental thermodynamic properties of DOX-HCl drug adsorption onto CS-co-pAA-GAR)/MWCNTs nanocomposite were estimated by calculating X_m values at various solution temperatures. As depicted in **Figure 14** (plot of ln K_d and reciprocal absolute temperature), the enthalpy (ΔH), entropy (ΔS), and Gibbs free energy (ΔG) changes were determined using Equations (3-5) as [59-61]:

$$\Delta G = \Delta H - T.\Delta S \quad (3)$$

$$\Delta G = -RT \ln K_{eq} \quad (4)$$

$$\ln Keq = -\frac{\Delta H}{RT} + \frac{\Delta S}{R} \quad (5)$$

Table 4 presents parameters for surface adsorption of DOX-HCl drug as a function of temperature. The negative Gibbs free energy (ΔG) for CS-co-pAA-GAR/MWCNTs nanocomposite confirm that adsorption is spontaneous [62]. Furthermore, the enthalpy value is less than 40 kJ/mol, and since the adsorption process is exothermic, this strongly suggests that DOX-HCl primarily adsorbs onto the nanocomposite surface through

physical means. The negative decrease in entropy (ΔS) indicates that the adsorbed particles on the polymer adsorbent surface become less mobile and more organized after the adsorption process [31, 63].

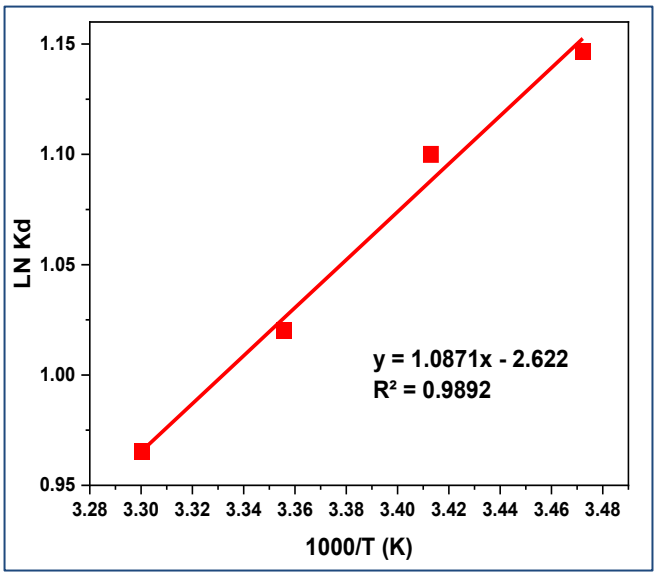

Figure 14. Plot showing the relationship between Ln K_d and reciprocal absolute temperature for DOX-HCl drug adsorption

Table 4. Thermal values for DOX-HCl drug adsorption

T (K)	ΔG (kJ/mol)	ΔH (kJ/mol)	ΔS (J/mol.K)
288	-2.759	-9.0381	-21.7993
293	-2.650		
298	-2.541		
303	-2.432		

3.5. Adsorption kinetics

Analyzing the kinetic process of adsorption necessitates understanding the reaction dynamics and investigating the specific adsorption conditions. Various kinetic models have been employed to evaluate experimental data, aiming to elucidate the adsorption mechanism and identify the rate-controlling step. To determine the kinetic equation governing the adsorption process, several models were utilized, including pseudo-first-order, and pseudo-second-order kinetic models. The pseudo-first-order kinetic model, for instance, is represented by Equation 6 [64, 65] as:

$$\text{Ln}\,(q_e - q_t) = \ln(q_e) - k_1 \cdot t. \quad (6)$$

The ln (q_e - q_t) linear plot is shown as a function of time (t). **Table 5** and **Figure 15a** contain pertinent data about DOX-HCl. The rate at which adsorbent's active participants are filled is directly proportional to quantity of vacant spaces, as per pseudo-first-order kinetic model. According to the pseudo-second-order model, the sharing or exchange of electrons between the adsorbent and adsorbate controls the rate of surface adsorption. The Equation (7) represents pseudo-second-order model [52, 56].

$$\frac{1}{q} = \frac{1}{k2.qe2} + \frac{t}{qe} \quad (7)$$

The constant k_2 is defined as a pseudo-second-order rate constant (g.mg^{-1} min^{-1}) (56, 59-61).

The calculated values for equilibrium adsorption capacity (q_e) and the pseudo-second-order rate constant (k_2) for DOX-HCl adsorption onto CS-co-pAA-GAR/MWCNTs nanocomposite are presented in **Table 5** and **Figure 15b.** These values were estimated from intercept and slope of plotted lines at various DOX-HCl concentrations. The kinetics of DOX-HCl adsorption by CS-co-pAA-GAR/MWCNTs nanocomposite appear

to be well-described by pseudo-second-order equation. This is evident from close agreement between calculated adsorption capacity (q_{cal}) and the experimentally observed adsorption capacity (q_{exp}). Consequently, this model consistently provides a higher correlation coefficient compared to other kinetic models [66-68].

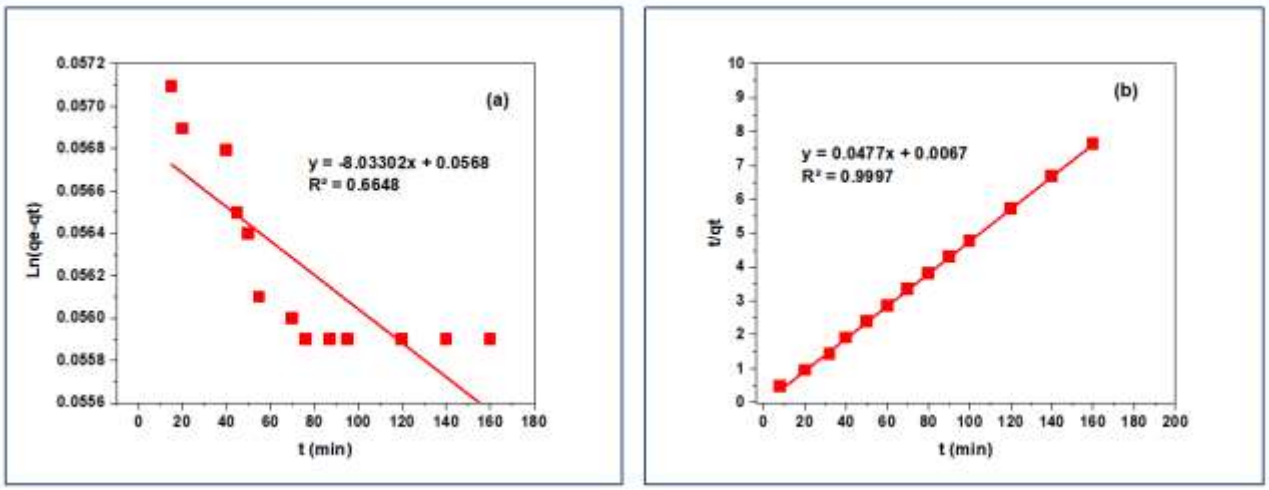

Figure 15. (a) Pseudo first order and (b) pseudo second order of DOX-HCl drug adsorption

Table 5. Pseudo first and pseudo second order model of DOX-HCl drug adsorption

Pseudo-first order			Pseudo-second order			
K_1 (1/min)	q_e (cal) (mg/g)	R^2	K_2	q_e (cal) (mg/g)	h	R^2
8.03302	1.057	0.6648	0.346	20.96436	152.1	0.9997

4. Conclusion

Incorporating garlic powder into (CS-co-pAA-GAR/MWCNTs) nanocomposite significantly enhanced its biological performance, particularly its antibacterial and antioxidant properties. This beneficial effect is attributed to the presence of active compounds like Allicin. Previous studies have consistently shown that garlic possesses broad-spectrum antimicrobial activity, further supporting the potential of this composite for various medical and environmental applications[69-71]. The successful synthesis of CS-co-pAA-GAR/MWCNTs nanocomposite was demonstrated, along with its efficient use for the adsorption of DOX-HCl from aqueous solutions. The Freundlich and pseudo second order adsorption models effectively described this process indicating the nanocomposite's high capacity and favorable adsorption characteristics for DOX-HCl. Optimal adsorption conditions were determined to be a contact time of 90 minutes, an initial adsorbate concentration of 100 mg/L, and a pH of 6 at 293 K. Furthermore, the thermodynamic parameters, with negative values for Gibbs free energy ($\Delta G = -2.650$ kJ/mol), enthalpy ($\Delta H = -9.0381$ kJ/mol), and entropy ($\Delta S = -21.7993$ J/mol·K), collectively confirm that the adsorption process is exothermic and spontaneous.

Conflict of interest

The authors declare there is no conflict of interest.

References

1. Al-Harbi LM, Alsulami QA, Farea M, Rajeh A. Tuning optical, dielectric, and electrical properties of Polyethylene oxide/Carboxymethyl cellulose doped with mixed metal oxide nanoparticles for flexible electronic devices. Journal of Molecular Structure. 2023;1272:134244.
2. Al-Hazmi GH, Refat MS, Alshammari KF, Kubra KT, Shahat A. Efficient toxic doxorubicin hydrochloride removal from aqueous solutions using facial alumina nanorods. Journal of Molecular Structure. 2023;1272:134187.

3. Fadhil HA, Samir AH, Mohammed YA, Al Rubaei Z. Synthesis, characterization, and in vitro study of novel modified reduced graphene oxide (RGO) containing heterocyclic compounds as anti-breast cancer. Eurasian Chem Commun. 2022;4:1156.
4. Khandaker S, Toyohara Y, Saha GC, Awual MR, Kuba T. Development of synthetic zeolites from bio-slag for cesium adsorption: Kinetic, isotherm and thermodynamic studies. Journal of Water Process Engineering. 2020;33:101055.
5. Alam M, Uddin M, Asiri AM, Awual MR, Fazal M, Rahman MM, et al. Fabrication of selective L-glutamic acid sensor in electrochemical technique from wet-chemically prepared RuO2 doped ZnO nanoparticles. Materials Chemistry and Physics. 2020;251:123029.
6. Rahman MM, Alamry KA, Awual MR, Mekky AE. Efficient Hg (II) ionic probe development based on one-step synthesized diethyl thieno [2, 3-b] thiophene-2, 5-dicarboxylate (DETTDC2) onto glassy carbon electrode. Microchemical Journal. 2020;152:104291.
7. Zhang M, Jiang L. Doxorubicin hydrochloride-loaded mesoporous silica nanoparticles inhibit non-small cell lung cancer metastasis by suppressing VEGF-mediated angiogenesis. Journal of biomedical nanotechnology. 2016;12(11):1975-86.
8. Guan X, Li Y, Jiao Z, Chen J, Guo Z, Tian H, et al. A pH-sensitive charge-conversion system for doxorubicin delivery. Acta Biomaterialia. 2013;9(8):7672-8.
9. Vallet-Regí M, Colilla M, Izquierdo-Barba I, Manzano M. Mesoporous silica nanoparticles for drug delivery: Current insights. Molecules. 2017;23(1):47.
10. Tacar O, Sriamornsak P, Dass CR. Doxorubicin: an update on anticancer molecular action, toxicity and novel drug delivery systems. Journal of pharmacy and pharmacology. 2013;65(2):157-70.
11. Octavia Y, Tocchetti CG, Gabrielson KL, Janssens S, Crijns HJ, Moens AL. Doxorubicin-induced cardiomyopathy: from molecular mechanisms to therapeutic strategies. Journal of molecular and cellular cardiology. 2012;52(6):1213-25.
12. Toledano-Medina MA, Pérez-Aparicio J, Moreno-Rojas R, Merinas-Amo T. Evolution of some physicochemical and antioxidant properties of black garlic whole bulbs and peeled cloves. Food chemistry. 2016;199:135-9.
13. Shao X, Sun C, Tang X, Zhang X, Han D, Liang S, et al. Anti-inflammatory and intestinal microbiota modulation properties of Jinxiang garlic (Allium sativum L.) polysaccharides toward dextran sodium sulfate-induced colitis. Journal of Agricultural and Food Chemistry. 2020;68(44):12295-309.
14. Kim JH, Nam SH, Rico CW, Kang MY. A comparative study on the antioxidative and anti-allergic activities of fresh and aged black garlic extracts. International Journal of Food Science and Technology. 2012;47(6):1176-82.
15. Ali MM, Mhaibes RM, Othman MAM, Lahhob QR, Qasim MJ. Association between triglyceride-glucose index and risk of chronic kidney disease: a systematic review and meta-analysis. Journal of Nephropharmacology. 2024;13(2).
16. AlSaadi EK, Darweesh MA, Al Jawadi HF, Othman MAM. Demographic Characteristics, Clinical Features, Laboratory, and Radiological Findings in Children Admitted to COVID19 Center in Amara City, Misan Province, Iraq. Journal of Medicinal and Chemical Sciences. 2023;6(1):34-43.
17. Correa MJ, Burbano Moreano JJ, Guardianelli LM, Weisstaub AR, Zuleta A, Salinas MV. Garlic: A natural bread improver for wheat bread with a high level of resistant starch. Journal of Food Processing and preservation. 2021;45(6):e15519.
18. Thuy BTP, My TTA, Hai NTT, Hieu LT, Hoa TT, Thi Phuong Loan H, et al. Investigation into SARS-CoV-2 resistance of compounds in garlic essential oil. ACS omega. 2020;5(14):8312-20.
19. Chen J, Huang G. Antioxidant activities of garlic polysaccharide and its phosphorylated derivative. International Journal of Biological Macromolecules. 2019;125:432-5.
20. Daliri EB-M, Ofosu FK, Chelliah R, Oh D-H. Lacto-fermented and unfermented soybean differently modulate serum lipids, blood pressure and gut microbiota during hypertension. Fermentation. 2023;9(2):152.
21. Al-Suraify SMT. Synthesis and characterization of novel compounds derived from 6-methyl-2,6 dihydro[1,2,4-triazino[4,3-b] indazol-3(4h)-one. International Journal of Pharmaceutical Research. 2020;12:1504-17.
22. Al-Suraify SMT. Synthesis and characterization of new heterocyclic compounds in corporating heterocyclic moiety derived from 3-chloro-1-methyl-1h-indazole. Biochemical and Cellular Archives. 2020;20:4127-34.
23. Al-Suraify SMT, Mekky AH, Husssien LB. Synthesis of new nitrogenous derivatives based on 3-chloro–1-methyl-1H-indazole. International Journal of Pharmaceutical Research. 2020;12:793-802.
24. Al-Suraify SMT, Hussien LB. Synthesis and characterization of new compounds derived from 1H-indol-5-ylamine. Applied Nanoscience (Switzerland). 2023;13(3):2083-92.
25. Shang A, Cao S-Y, Xu X-Y, Gan R-Y, Tang G-Y, Corke H, et al. Bioactive compounds and biological functions of garlic (Allium sativum L.). Foods. 2019;8(7):246.
26. Bakrim S, El Menyiy N, Moubachir R, Taha D, Bouyahya A, Mubarak MS. Major Bioactive Compounds 4 and Antidiabetic Activity of Allium sativum. Antidiabetic Medicinal Plants and Herbal Treatments: CRC Press; 2023. p. 63-73.
27. Chung LY. The antioxidant properties of garlic compounds: allyl cysteine, alliin, allicin, and allyl disulfide. Journal of medicinal food. 2006;9(2):205-13.

28. Hamed HS, Ismal SM, Faggio C. Effect of allicin on antioxidant defense system, and immune response after carbofuran exposure in Nile tilapia, Oreochromis niloticus. Comparative Biochemistry and Physiology Part C: Toxicology & Pharmacology. 2021;240:108919.
29. Khudair ZJ, Kadam ZM. Physicochemical Characterization of Chitosan-Multiwalled Carbon Nanotubes Hybrid Material for Ofloxacin Delivery. Indonesian Journal of Chemistry.
30. Meng J, Wang Z-G, Zhao X, Wang Y, Chen D-Y, Liu D-L, et al. Silica nanoparticle design for colorectal cancer treatment: Recent progress and clinical potential. World Journal of Clinical Oncology. 2024;15(6):667.
31. Khudair ZJ, Kadam Z. Adsorption behavior of Chitosan-MWCNTS nanocomposite for the elimination of ofloxacin medication. Chem J Mold. 2024;19(1):84-92.
32. Shah A, Arjunan A, Manning G, Batool M, Zakharova J, Hawkins AJ, et al. Sequential novel use of Moringa oleifera Lam., biochar, and sand to remove turbidity, E. coli, and heavy metals from drinking water. Cleaner Water. 2024;2:100050.
33. Shah A, Arjunan A, Thumma A, Zakharova J, Bolarinwa T, Devi S, et al. Adsorptive removal of arsenic from drinking water using KOH-modified sewage sludge-derived biochar. Cleaner Water. 2024;2:100022.
34. Shah A, Zakharova J, Batool M, Coley MP, Arjunan A, Hawkins AJ, et al. Removal of cadmium and zinc from water using sewage sludge-derived biochar. Sustainable Chemistry for the Environment. 2024;6:100118.
35. Mahdi MA, Jasim LS, Mohamed MH. Synthesis and anticancer activity evaluation of novel ligand 2- [2 - (5-Chloro carboxy phenyl) Azo] 1-Methyl Imidazole (1-Mecpai) with Some Metal Complexes. Systematic Reviews in Pharmacy. 2020;11(12):1979-87.
36. Jamel HO, Jasim MH, Mahdi MA, Ganduh SH, Batool M, Jasim LS, et al. Adsorption of Rhodamine B dye from solution using 3-((1-(4-((1H-benzo[d]imidazol-2-yl)amino)phenyl)ethylidene)amino)phenol (BIAPEHB)/ P(AA-co-AM) composite. Desalination and Water Treatment. 2025;321.
37. Majeed HJ, Idrees TJ, Mahdi MA, Abed MJ, Batool M, Yousefi SR, et al. Synthesis and application of novel sodium carboxy methyl cellulose-g-poly acrylic acid carbon dots hydrogel nanocomposite (NaCMC-g-PAAc/CDs) for adsorptive removal of malachite green dye. Desalination and Water Treatment. 2024;320:100822.
38. Alshamusi QKM, Alzayd AAM, Mahdi MA, Jasim LS, Aljeboree AM. ADSORPTION OF CRYSTAL VIOLATE (CV) DYE IN AQUEOUS SOLUTIONS BY USING P(PVP-CO-AAM)/GO COMPOSITE AS (ECO-HEALTHY ADSORBATE SURFACE): CHARACTERIZATION AND THERMODYNAMICS STUDIES. Biochemical and Cellular Archives. 2021;21:2423-31.
39. Abdulsahib WK, Sahib HH, Mahdi MA, Jasim LS. Adsorption Study of Cephalexin Monohydrate Drug in Solution on Poly (vinyl pyrrolidone-acryl amide) Hydrogel Surface. International Journal of Drug Delivery Technology. 2021;11(4):1169-72.
40. Kianipour S, Razavi FS, Hajizadeh-Oghaz M, Abdulsahib WK, Mahdi MA, Jasim LS, et al. The synthesis of the P/N-type NdCoO3/g-C3N4 nano-heterojunction as a high-performance photocatalyst for the enhanced photocatalytic degradation of pollutants under visible-light irradiation. Arabian Journal of Chemistry. 2022;15(6).
41. Mahdi MA, Oroumi G, Samimi F, Dawi EA, Abed MJ, Alzaidy AH, et al. Tailoring the innovative Lu2CrMnO6 double perovskite nanostructure as an efficient electrode materials for electrochemical hydrogen storage application. Journal of Energy Storage. 2024;88.
42. Radhy ND, Jasim LS. A novel economical friendly treatment approach: Composite hydrogels. Caspian Journal of Environmental Sciences. 2021;19(5):841-52.
43. Batool M, Haider MN, Javed T. Applications of spectroscopic techniques for characterization of polymer nanocomposite: A review. Journal of Inorganic and Organometallic Polymers and Materials. 2022;32(12):4478-503.
44. Mohammad HA, Mahde BW, Jasim LS, Batool M. Adsorption of Diclofenac Sodium (DS) Drug from Water on CMC-gP (AAc-AAm) Nano-Hydrogel: Isotherm and Thermodynamic Study. Journal of Nanostructures. 2024;14(1):232-44.
45. Karim AN, Jasim LS. Synthesis and characterization of poly (CH/AA-co-AM) composite: Adsorption and thermodynamic studies of benzocaine on from aqueous solutions. International Journal of Drug Delivery Technology. 2019;9(4):558-62.
46. Whaib HA, Kadam ZM, editors. Synthesis and characterization of a nano reagent and its use as a new type to inhibit alkaline phosphate enzyme, the study of the enzyme's inhibitory kinetic properties and the study of its biological activity. AIP Conference Proceedings; 2023: AIP Publishing LLC.
47. Alwan NA, Kadam ZM, editors. Preparing and diagnosing the biological activity of some metallic complexes with ligand 4-Benzophenol Azopyrogallol (4). IOP Conference Series: Earth and Environmental Science; 2021: IOP Publishing.
48. Roney C, Kulkarni P, Arora V, Antich P, Bonte F, Wu A, et al. Targeted nanoparticles for drug delivery through the blood–brain barrier for Alzheimer's disease. Journal of controlled release. 2005;108(2-3):193-214.
49. Haider MN. Enhanced Degradation of reactive violet 1 (RV1) Dye Using Gamma and UV Irradiation Coupled with Hydrogen Peroxide. Radiation Physics and Chemistry. 2025:113191.
50. Zeeshan M, Javed T, Kumari C, Thumma A, Wasim M, Taj MB, et al. Investigating the Interactions between Dyes and Porous/Composite Materials: A Comprehensive Study. Sustainable Chemistry for the Environment. 2025:100217.

51. Singh AK, Mishra SK, Mishra G, Maurya A, Awasthi R, Yadav MK, et al. Inorganic clay nanocomposite system for improved cholinesterase inhibition and brain pharmacokinetics of donepezil. Drug Development and Industrial Pharmacy. 2020;46(1):8-19.
52. Arshad R, Javed T, Thumma A. Exploring the efficiency of sodium alginate beads and Cedrus deodara sawdust for adsorptive removal of crystal violet dye. Journal of Dispersion Science and Technology. 2024;45(12):2330-43.
53. Wang Z, Zhang Z, He C, Wang Q. Advances in the application of hydrogel adhesives for wound closure and repair in abdominal digestive organs. Biomaterials Science. 2025;13(10):2606-27.
54. Mohammad HA, Mahde BW, Jasim LS, Batool M. Adsorption of Diclofenac Sodium (DS) Drug from Water on CMC-g-P(AAc-AAm) Nano-Hydrogel: Isotherm and Thermodynamic Study. Journal of Nanostructures. 2024;14(1):232-44.
55. Mojar Alshamusi QK, Hameed KAA, Taher AM, Batool M, Jasim LS. Efficiency of Chitosan-Grafted Poly (Carboxymethyl Cellulose-Co-Acrylamide) Nano Hydrogel for Cadmium (II) Removal: Batch Adsorption Study. Journal of Nanostructures. 2024;14(4):1122-33.
56. Javed T, Kausar F, Zawar MD, Khalid N, Thumma A, Ismail A, et al. Investigating the adsorption potential of coconut coir as an economical adsorbent for decontamination of lanthanum ion from aqueous solution. Journal of Dispersion Science and Technology. 2024.
57. Taher A, Jasim LS, Mehmood Z, Zawar MD, Haider MN, Batool M. Applications of Nano Composites for Heavy Metal Removal from Water by Adsorption: Mini Review. Journal of Nanostructures. 2024;14(4):1239-51.
58. Neamah Thamer A, S. Alwan A, A. Alwan N, Jasim LS, Batool M. Adsorptive removal of chromium (Cr (III)) and lead (Pb (II)) ions from water using crosslinked polyvinyl alcohol-acrylamide P (VA-AAm) hydrogel. International Journal of Environmental Analytical Chemistry. 2025:1-26.
59. Bukhari A, Javed T, Haider MN. Adsorptive exclusion of crystal violet dye from wastewater by using fish scales as an adsorbent. Journal of Dispersion Science and Technology. 2023;44(11):2081-92.
60. Imran MS, Javed T, Areej I, Haider MN. Sequestration of crystal violet dye from wastewater using low-cost coconut husk as a potential adsorbent. Water Science and Technology. 2022;85(8):2295-317.
61. Urooj H, Javed T, Taj MB, Nouman Haider M. Adsorption of crystal violet dye from wastewater on Phyllanthus emblica fruit (PEF) powder: kinetic and thermodynamic. International Journal of Environmental Analytical Chemistry. 2024;104(19):7474-99.
62. Wang D, Sun Y, Liu Y, Meng F, Lee RJ. Clinical translation of immunoliposomes for cancer therapy: Recent perspectives. Expert opinion on drug delivery. 2018;15(9):893-903.
63. N. Zghair A, T. Al-Khateeb Z, S. Jasim L, Batool M. Synthesis, characterization and adsorption properties of azo-functionalized polymeric hydrogels for R6G dye removal from water. Applied Chemical Engineering. 2025;8(1):ACE-5604.
64. Batool M, Javed T, Wasim M, Zafar S, Din MI. Exploring the usability of Cedrus deodara sawdust for decontamination of wastewater containing crystal violet dye. Desalination and Water Treatment. 2021;224:433-48.
65. Mutashar MO, Shahad RF, Jasim IS, Batool M. Removal of Pb (II) Ions from Water by Adsorption on Sodium Alginate-g-poly (Acrylic acid-co-Itaconic acid)/Titanium Dioxide [SA-gp (AA-IA)/TiO2] Hydrogel Nanocomposite. Journal of Nanostructures. 2025;15(3):983-96.
66. Abdulhusain ZH, Jasim LS, Batool M. Azur C Dye Removal using GO/P (CMC-Co-Am) Nanocomposite: Adsorption and Kinetic Studies. Journal of Nanostructures. 2024;14(4):1225-38.
67. Taher AM, Jasim LS, Mehmood Z, Zawar MD, Haider MN, Batool M. Applications of Nano Composites for Heavy Metal Removal from Water by Adsorption: Mini Review. Journal of Nanostructures. 2024;14(4):1239-51.
68. Saadallah K, AD C, Djedid M, Batool M, Benalia M, Saadallah S, et al. Potential of the Algerian pine tree bark for the adsorptive removal of methylene blue dye: Kinetics, isotherm and mechanism study. Journal of Dispersion Science and Technology. 2024:1-19.
69. Ankri S, Mirelman D. Antimicrobial properties of allicin from garlic. Microbes and infection. 1999;1(2):125-9.
70. Amagase H, Petesch BL, Matsuura H, Kasuga S, Itakura Y. Recent advances on the nutritional effects associated with the use of garlic as a supplement. J Nutr. 2001;131(3):955S-62S.
71. Bayan L, Koulivand PH, Gorji A. Garlic: a review of potential therapeutic effects. Avicenna journal of phytomedicine. 2014;4(1):1.
72. Tariq Z, Alwan NA. Optimization of Switchable Hydrophilicity Solvent-Based Liquid-Liquid Microextraction for Tartrazine Dye Separation and Preconcentration using Central Composite Design and Response Surface Methodology. Methods and Objects of Chemical Analysis. 2024;19(4):200-5.